

Nuclear spirals in galaxies: gas response to asymmetric potential. I. Linear theory

Witold Maciejewski

Observatorium Astronomiczne Uniwersytetu Jagiellońskiego, ul. Orła 171, 30-244 Kraków, Poland

10 November 2018

ABSTRACT

Nuclear spirals can provide a wealth of information about the nuclear potential in disc galaxies. They are unlikely to form in nuclei with solid-body rotation, yet they are present in a majority of galactic centres. Their morphology varies depending on whether a central massive black hole (MBH) is present or absent in the galaxy. In this paper I consider predictions of the linear theory for waves induced in gas by asymmetric gravitational potential, which are applicable to the nuclear spirals observed in galaxies. Generation and propagation of waves is governed by dynamical resonances, and inclusion of a MBH can move or even create resonances, greatly altering the extent and shape of the nuclear spiral. I will use predictions of the linear theory presented here as a guideline when interpreting hydrodynamical models in the second paper of this series. I also comment on modifications that self-gravity in gas imposes on the induced waves.

Key words: galaxies: kinematics and dynamics — galaxies: ISM — galaxies: spiral — galaxies: structure — galaxies: nuclei — ISM: kinematics and dynamics

1 INTRODUCTION

Recent high-resolution maps of galactic centres reveal intricate dust structures, which are often organized in a clear spiral pattern. The surveys by Regan & Mulchaey (1999), Martini & Pogge (1999), Pogge & Martini (2002), and Martini et al. (2003 a,b) indicate that 50% to 80% of galaxies in their samples possess such *nuclear spirals*, regardless of their nuclear activity. The pattern of some nuclear spirals is highly organized, like in grand-design spirals in the main galactic discs. Such nuclear spirals, often winding by more than a 2π angle, seem to connect smoothly at their outer end to the straight dust lanes in the galactic bar, and sometimes to the outer spiral arms in the main galactic disc. Other nuclear spirals are more chaotic or flocculent.

Martini & Pogge (1999) estimated gas density in the nuclear spirals, and showed that they reside in not self-gravitating gaseous discs. Therefore the standard Lin-Shu theory (Lin & Shu 1964, 1966), which explains formation of a grand-design spiral structure in the main galactic discs, does not apply to them. Flocculent nuclear spirals may result from acoustic noise (Elmegreen et al. 1998, Montenegro, Yuan & Elmegreen 1999), while more regular ones are likely to form as a gas response to the asymmetry in the gravitational potential. Here I explore this last scenario.

The theory of gaseous density waves responsive to a rigidly rotating external potential has been developed by Goldreich & Tremaine (1978, 1979) in the linear approximation. They showed that the propagation of the waves

strongly depends on the resonances created by the rotating asymmetric potential. This theory was first applied by Lindblad & Jörsäter (1981) to the spiral structure in the nucleus of the barred galaxy NGC 1512, where such a structure has been described and analyzed for the first time, and the term ‘nuclear spiral’ has been introduced. Yuan & Cheng (1989, 1991) proposed a nonlinear version of this wave theory, which has been then applied by Yuan & Kuo (1997) to study waves generated at various resonances. Englmaier & Shlosman (2000) confronted the results of the linear theory with the high-resolution hydrodynamical modeling, showing that gaseous nuclear spirals which form in their models of barred galaxies can be understood in terms of the linear theory of waves in gas generated by asymmetric potential.

The shape of nuclear spiral depends on the properties of the nuclear gravitational potential, as originally noticed by Englmaier & Shlosman, though constraints that they put on the frequency curve generate rotation curves with particular behaviour near the galactic centre ($d\Omega/dR \rightarrow R^{-1}$). Such rotation curve cannot represent the commonly assumed solid-body rotation of galactic centres, nor it can account for the presence of a massive black hole (MBH) in the galactic centre. In this paper, I study the linear prediction of the shape and extent of nuclear spirals in a wider range of galactic potentials, and of their corresponding rotation curves. I focus on the potentials that are either commonly assumed (inner solid-body rotation), or recently recognized (central MBH). The evidence is growing for such MBHs from clear kinemat-

arXiv:astro-ph/0408098v1 4 Aug 2004

ical indications of large concentrations of dark mass in the very centres of galaxies (see e.g. Kormendy & Gebhardt 2001 for a recent review). A central MBH governs the resonances beyond its classically defined sphere of influence¹, and can significantly modify the appearance of the nuclear spiral. I also consider a power-law density distribution in the galactic centre, which seems to fit the rotation curve of our Galaxy remarkably well (Dehnen & Binney 1998).

For consistency, I outline in Section 2 the derivation of the basic formulae in the linear theory of gaseous density waves generated by a rigidly rotating external potential, when self-gravity in gas is included. As a first approximation, I neglect this self-gravity in Section 3, where characteristics of nuclear spirals in various galactic gravitational potentials are calculated. Corrections for self-gravity in gas are analyzed in Section 4. The linear prediction for non-selfgravitating gas will serve as a framework when analyzing hydrodynamical models of nuclear spirals in the second paper of the series (Maciejewski 2004, Paper II).

2 BASIC EQUATIONS OF THE LINEAR DENSITY-WAVE THEORY

2.1 The dispersion relation

Formation and survival of spiral structure in disc galaxies is commonly explained by the density-wave theory for self-gravitating discs (Lin-Shu theory; Lin & Shu 1964, 1966; see also Binney & Tremaine 1987, pp.347–359). Contrary to the main galactic disc, where the dynamics of gas and stars is strongly coupled, gas in galactic central regions decouples from stars, which reside there mostly in the hot bulge, and settles in a dynamically cold disc. In each of these two cases, a different regime of wave propagation takes place: on large scales, the self-gravitating spiral itself is the perturbation in the potential of an otherwise axisymmetric disc, while on the nuclear scales the dynamics of the gaseous disc can be treated chiefly as a response to the driving from the stellar potential, with a correction for self-gravity in gas. Thus nuclear spirals can be explained as waves in the gaseous disc, generated by asymmetries in the stellar potential of the galaxy, and constitute *induced* density waves.

I list here the derivation of the equations governing the dynamics of gas in such a regime, appropriate for the galactic centres. Most of these equations have been originally obtained by Goldreich & Tremaine (1979), and canonized by Binney & Tremaine (1987, pp.352–359). Nonlinear solutions have been studied by Yuan & Kuo (1997) and Montenegro et al. (1999). Here I limit the theory to the derivation of equations that can be confronted with the numerical simulations in Paper II, and I point out the crucial limiting assumptions in this derivation. I also write these equations in the form allowing to see how self-gravity in gas modifies the results.

I assume here that gas in the disc is isothermal (derivation for a polytropic equation of state is analogous, see e.g. Binney & Tremaine, 1987). Then the gas density ρ is related

to the pressure P by a simple equation of state $P = c^2\rho$, where c is the sound speed in gas. With this equation of state, the equations of continuity and of motion take the form

$$\frac{\partial \rho}{\partial t} + \nabla \cdot (\rho \mathbf{v}) = 0, \quad (1)$$

$$\rho \frac{\partial \mathbf{v}}{\partial t} + \rho (\mathbf{v} \cdot \nabla) \mathbf{v} = -c^2 \nabla \rho - \rho \nabla \Phi, \quad (2)$$

where \mathbf{v} is gas velocity, Φ is the total gravitational potential, and other symbols have their usual meaning. Because of the symmetries in the problem, it is convenient to solve the above equations in cylindrical coordinates. Furthermore, let's assume that the disc is thin, and neglect changes perpendicular to the disc plane. This reduces the problem to two dimensions with ρ being now interpreted as the surface density of gas.

Equations (1) - (2) are highly nonlinear, but they can be linearized for gas flows slightly departing from the circular motion of axisymmetric gas distribution in axisymmetric potential. Thus at any location (R, φ) in the gaseous disc, one can expand all variables in (1) - (2) as a sum of the zeroth order axisymmetric term (hereafter indexed by 0), and a first order perturbation, hereafter indexed by 1. Moreover, note that the zeroth order of the radial gas velocity is $v_{R0} = 0$, and the tangential one can be written as $v_{\varphi 0} = R \frac{\partial \Phi_0}{\partial R} + \frac{Rc^2}{\rho_0} \frac{\partial \rho_0}{\partial R}$. The expansion of (1) takes a form:

$$\frac{\partial \rho_1}{\partial t} + \frac{\rho_0 v_{R1}}{R} + v_{R1} \frac{\partial \rho_0}{\partial R} + \rho_0 \frac{\partial v_{R1}}{\partial R} + \frac{\rho_0}{R} \frac{\partial v_{\varphi 1}}{\partial \varphi} + \Omega \frac{\partial \rho_1}{\partial \varphi} = 0, \quad (3)$$

where $\Omega = v_{\varphi 0}/R$.

The expansion of the components of (2) takes a particularly simple form when the gravitational potential Φ_1 and the gas density ρ_1 get combined to a single variable $H_1 = \Phi_1 + c^2 \frac{\rho_1}{\rho_0}$, and it can be written as

$$\frac{\partial v_{R1}}{\partial t} + \Omega \frac{\partial v_{R1}}{\partial \varphi} - 2\Omega v_{\varphi 1} = -\frac{\partial H_1}{\partial R}, \quad (4)$$

$$\frac{\partial v_{\varphi 1}}{\partial t} + \Omega \frac{\partial v_{\varphi 1}}{\partial \varphi} - 2Bv_{R1} = -\frac{1}{R} \frac{\partial H_1}{\partial \varphi}, \quad (5)$$

where $B = -\frac{1}{2} \left[\frac{\partial(\Omega R)}{\partial R} + \Omega \right]$ is the Oort parameter, which is related to the epicyclic frequency κ by $\kappa^2 = -4B\Omega$.

Each perturbation X_1 (i.e. Φ_1 , v_{R1} , etc.) can be expanded as a sum of terms, which can be written as

$$Re [X_a(R) e^{i(m\varphi - \omega t)}] \quad \text{or} \quad Re [X_a(R) e^{im(\varphi - \Omega_P t)}], \quad (6)$$

where m is positive only and accounts for geometry, and ω indicates patterns that rotate with respect to the inertial frame with angular frequency $\Omega_P = \omega/m$. With this expansion, (3) - (5) can be rewritten as

$$i\rho_a m(\Omega - \Omega_P) + \frac{1}{R} \frac{d}{dR} [R\rho_0 v_{Ra}] + \frac{im\rho_0}{R} v_{\varphi a} = 0, \quad (7)$$

$$iv_{Ra} m(\Omega - \Omega_P) - 2\Omega v_{\varphi a} = -\frac{dH_a}{dR}, \quad (8)$$

$$iv_{\varphi a} m(\Omega - \Omega_P) - 2Bv_{Ra} = -\frac{1}{R} imH_a. \quad (9)$$

There are four unknowns in the system of equations (7) - (9): the density of gas ρ_a , its two velocity components v_{Ra} and $v_{\varphi a}$, and the gravitational potential from the gas Φ_{aG} , which contributes to the total potential Φ_a in H_a . Φ_{aG} is

¹ the sphere of influence of a MBH is defined by radius GM_{MBH}/σ^2 , where σ is the characteristic stellar velocity dispersion in the host galaxy; this definition is different from the one used in celestial mechanics

related to the gas density ρ_a by Poisson's equation, which closes the system (7) – (9). A common approach to solving this system is to get from (8) and (9) explicit formulae for v_{Ra} and $v_{\varphi a}$ in terms of H_a ,

$$\begin{aligned} v_{Ra} &= -i \frac{m(\Omega - \Omega_P) \frac{dH_a}{dR} + 2\Omega \frac{mH_a}{R}}{\kappa^2 - m^2(\Omega - \Omega_P)^2}, \\ v_{\varphi a} &= \frac{m(\Omega - \Omega_P) \frac{mH_a}{R} - 2B \frac{dH_a}{dR}}{\kappa^2 - m^2(\Omega - \Omega_P)^2}, \end{aligned} \quad (10)$$

and then to substitute these expressions in (7). As a result one gets a single differential equation, which together with Poisson's equation allows for a complete description of the response of a gaseous disc to the perturbation in gravitational potential, given that the resulting departures from circular motion are small. This equation has been analyzed in detail by Goldreich & Tremaine (1979), where it appears as eq.(13). Here I focus on its fundamental properties, and on the assumptions taken when deriving the dispersion relation from it.

All perturbations in (3) – (5) are of gas variables, except for H_1 on the right-hand sides of (4) and (5). H_1 involves perturbation from the imposed stellar potential Φ_{1S} , since

$$\Phi_1 = \Phi_{1G} + \Phi_{1S}, \quad (11)$$

where Φ_{1G} is the contribution from the self-gravity of the gaseous disc. In the absence of Φ_{1S} the problem reduces to the standard Lin-Shu theory (Lin & Shu 1964, 1966). On the other hand, the imposed potential Φ_{1S} introduces inhomogeneity in equations (3) – (5). In the approach taken here, all the perturbations entering these equations get expanded into components of the form (6). Thus, for each m and Ω_P one gets a corresponding set of equations in a component form (7) – (9). Note however that not all sets of these component equations are inhomogeneous: only terms with particular values of m and Ω_P are present in the expansion of Φ_{1S} . For example, if the imposed stellar potential comes from a bar rotating with a pattern speed Ω_B , then only terms with $\Omega_P = \Omega_B$ are present. Moreover, a bisymmetric bar decomposes into modes with only even m .

Thus all modes of perturbation in gas with m odd and $\Omega_P \neq \Omega_B$ propagate according to the standard Lin-Shu theory, i.e. they are self-excited, and not driven. In the case considered here, when the stellar potential dominates over the self-gravity in gas, these modes should be negligible compared to the driven ones. For the driven modes the component equations (7) – (9) are inhomogeneous: their regular solution consists of a free-wave part of the Lin-Shu theory, and of a forced non-wave part. However, this separation cannot be done around singularities in the solution. The formulae (10) for modes driven by the bar have singularities when $\kappa^2 - m^2(\Omega - \Omega_B)^2 = 0$. This happens when

$$\Omega_B = \Omega \pm \kappa/m, \quad (12)$$

that is at the Lindblad ($m : \pm 1$) resonances of the bar (in the notation of Sellwood & Wilkinson 1993). Perturbations are generated in gas there, and since modes with lowest m usually dominate in the expansion of the potential of the bar, the strongest waves are likely to be generated at ($2 : -1$) and ($2 : +1$) resonances, commonly called the inner Lindblad resonance (ILR) and the outer Lindblad resonance (OLR), respectively.

Away from the resonances, the solution can be separated into its wave and non-wave parts. The slowly changing non-wave part can be obtained in terms of the imposed stellar potential Φ_{1S} (see e.g. Goldreich & Tremaine 1979), but here we concentrate on the fast-changing free-wave part of the solution. For it, an analytic solution can be obtained when the perturbations $X_a(R)$ in (6) vary rapidly with radius ($X_a/R \ll dX_a/dR$). One can represent locally such variations as a plane-parallel wave-front with sinusoidal dependence on R :

$$X_a(R) = \bar{X} e^{ikR}, \quad (13)$$

where k is the wavenumber; for rapid variations $|kR| \ll 1$. Then $dX/dR = ikX$, and therefore in (7) the last term of the sum can be neglected, and only terms with the derivative remain in (10). After this truncation, substituting (10) into (7) returns

$$\rho_a [\kappa^2 - m^2(\Omega - \Omega_B)^2] - \frac{1}{R} \frac{d}{dR} \left[R \rho_0 \frac{dH_a}{dR} \right] = 0. \quad (14)$$

Note that in H_a , the perturbation Φ_{aS} from the extended stellar potential does not change rapidly with R , and therefore it does not contribute to the derivative. The derivatives of the two other contributions can be replaced by $ik\rho_a$, and $ik\Phi_{aG}$, which allows to write (14) as

$$\rho_a [\kappa^2 - m^2(\Omega - \Omega_B)^2] + k^2 \rho_0 \Phi_{aG} + k^2 c^2 \rho_a = 0, \quad (15)$$

where ρ_a and Φ_{aG} are related through Poisson's equation. For a plane-parallel wave in a thin disc, with the angular velocity changing on scales much larger than the radial wavelength of the wave, this equation simplifies to $-2|k|\Phi_{aG} = 4\pi G\rho_a$ (see e.g. Binney & Tremaine 1987, pp.310-312). This allows to eliminate Φ_{aG} from (15) and to get the dispersion relation

$$k^2 c^2 - 2\pi G|k|\rho_0 + \kappa^2 - m^2(\Omega - \Omega_B)^2 = 0 \quad (16)$$

for density waves in a gaseous disc of density ρ_0 driven by an external potential tumbling with a pattern speed Ω_B . Although the form of this relation is identical to that for the free density waves, the driven modes can only have pattern speed equal to that of the driver, with the multiplicity m that is present in the decomposition of the driving potential.

In deriving the dispersion relation (16), it has been assumed that a thin gaseous disc is a subject to wave-like perturbations that vary rapidly with radius, and that locally can be approximated by a plane-parallel wave, whose wavelength is much smaller than the scale of radial changes in the angular velocity of the disc.

2.2 Nuclear spirals as morphology of density waves

The linear theory describes waves propagating in a gaseous disc that are represented locally by (13). The simplest global counterpart of this local representation is a set of concentric rings in a rigidly rotating disc, and in a differentially rotating disc the advection of wave packets gives rise to a tightly wound spiral.

In polar coordinates (R, φ) the shape of any spiral curve can be described by equation $\varphi = g(R)$. If there is m identical arms, then also $\varphi + 2\pi l/m = g(R)$ for any $1 < l < m$, or, equivalently,

$$m\varphi = f(R). \quad (17)$$

If this m -arm spiral rotates with an angular speed Ω_P , it is described by $m(\varphi - \Omega_P t) = f(R)$. Now, let this spiral curve define locations of maxima for some density perturbation ρ_1 , which enters (3). The functional form for such a perturbation can then be written as

$$\begin{aligned} \rho_1(R) &= \text{Re} \left[H(R) e^{im(\varphi - \Omega_P t) - if(R)} \right] \\ &\simeq \text{Re} \left[H(R_0) e^{-if(R_0)} e^{ik(R_0)(R - R_0)} e^{im(\varphi - \Omega_P t)} \right], \end{aligned} \quad (18)$$

if the pattern is tightly wound. Here $H(R)$ is a slowly-varying function of radius. The last expression uses the expansion of $f(R)$ around R_0 , where

$$k(R) = -df(R)/dr. \quad (19)$$

Formula (18) conveys the density perturbation in the form (6) and (13) used in the derivation of the dispersion relation (16). In particular, $\rho_a = H(R_0) e^{-if(R_0)} e^{ik(R_0)(R - R_0)}$ and $\bar{\rho} = H(R_0) e^{-if(R_0)}$.

The wavenumber k is related to the radial wavelength λ by $\lambda = 2\pi/|k|$, which is also the radial separation between two adjacent arms. The pitch angle i of the spiral is given by $\cot i = R d\varphi/dR$, which from differentiating (17), and after substituting (19) gives

$$\cot i = \frac{|k|R}{m}. \quad (20)$$

3 DENSITY WAVES WITHOUT SELF-GRAVITY IN GAS

3.1 Regions permitting wave propagation

If the gas in the disc is not self-gravitating, then $\Phi_{aG} \equiv 0$, and the term with $|k|$ in (16) disappears, allowing for a simple and easy-to-interpret solution for k :

$$k = \pm \frac{m}{c} \sqrt{(\Omega + \kappa/m - \Omega_B)(\Omega - \kappa/m - \Omega_B)}. \quad (21)$$

The waves can propagate when k is real, and for k imaginary they decay. The wavenumber k is real when $\Omega + \kappa/m > \Omega_B$ and $\Omega - \kappa/m > \Omega_B$, or when $\Omega + \kappa/m < \Omega_B$ and $\Omega - \kappa/m < \Omega_B$. Furthermore, since by convention Ω and κ are positive, this condition for propagation of induced density waves gets simplified to

$$\Omega - \kappa/m > \Omega_B \quad \text{or} \quad \Omega + \kappa/m < \Omega_B. \quad (22)$$

Thus in galaxies with Ω monotonically decreasing (which is a reasonable rough assumption) density waves can propagate inside the ($m : -1$) Lindblad resonance and outside the ($m : +1$) one. Generally, in order to find the zones where density waves can propagate, the two sides of each inequality in (22) can be plotted as two separate functions of radius R and compared (Fig.1): Ω_B is an arbitrary constant pattern speed, and Ω and κ are derivatives of the rotation curve.

Here I focus on the first inequality in (22), which indicates a region located inside the corotation of the rotating asymmetric potential, i.e. where it is expected that nuclear spirals develop. The second inequality in (22) is satisfied outside the corotation, further from the galactic centre. The most typical asymmetry in the galactic stellar potential is a bisymmetric bar-like mode (Sellwood & Wilkinson 1993,

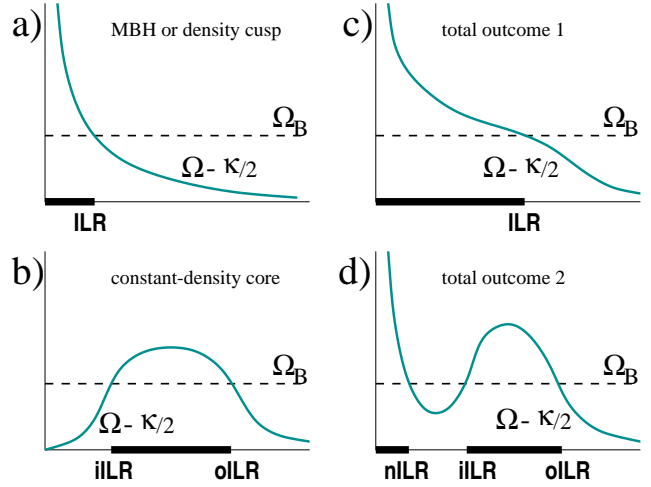


Figure 1. Typical frequency curves (frequency in usual units of time^{-1} plotted against radius) for various gravitational potentials of: **a)** a MBH or a continuous mass distribution with a central density cusp, **b)** continuous mass distribution with a constant-density core (linear rise of the inner rotation curve), **c)** first variant of a composite frequency curve: monotonous decline, **d)** second variant: composite frequency curve with multiple extrema. Regions where induced density waves can propagate are indicated by thick lines on the horizontal axis. Resonances are labeled under the axis (see text).

Eskridge et al. 2001), for which $m = 2$. This mode generates density waves inside its corotation when $\Omega - \kappa/2 > \Omega_B$. The $\Omega - \kappa/2$ curve, being bound from the top by Ω , always declines towards zero at large radii. Since

$$\kappa = 2\Omega \sqrt{1 + \frac{R}{2\Omega} \frac{d\Omega}{dr}}, \quad (23)$$

the $\Omega - \kappa/2$ curve cannot be negative, unless the angular velocity increases with radius. Interestingly, contrary to any other m , for $m = 2$ the condition $\Omega - \kappa/m = \Omega_B$ can be fulfilled at more than one radii, i.e. the galaxy can have more than one ILR.

In order to see how the number of ILRs depends on the underlying gravitational potential, take an example of a power-law rotation curve $\Omega = Ar^B$. In this case $\kappa = 2\Omega \sqrt{1 + B/2}$, and $\Omega - \kappa/2$ is proportional to the angular velocity Ω . Thus the $\Omega - \kappa/2$ curve reaches infinity in the galactic centre when the galaxy mass is sufficiently centrally concentrated or when a central massive black hole (MBH) is present there ($B = -3/2$). This situation is illustrated in Fig.1a. However, when $B = 0$ at the innermost radii, i.e. when the inner parts of the galaxy approach solid-body rotation, characteristic for a constant-density core, $\Omega - \kappa/2$ decreases inwards to zero (Fig.1b), because $\Omega - \kappa/2 \equiv 0$ for $\Omega = \text{const}$. Combining the contribution from the MBH (or the central mass concentration) with that of the stellar potential (that may possibly include a constant-density core), one can obtain two different composite shapes of the $\Omega - \kappa/2$ curve: one with a single ILR (Fig.1c), and one with three ILRs (Fig.1d): the nuclear ILR (nILR), the inner ILR (iILR), and the outer ILR (oILR). The first composite shape occurs when there is no linear rise in the central rotation

curve, or if this rise is overcome by the contribution from the central mass concentration. Then the density wave can propagate all the way from the single ILR to the galactic centre. The second composite shape indicates an extensive constant-density core resulting in solid-body rotation. Note that even here I assume the presence of a MBH in the centre, which causes the innermost rise of the $\Omega - \kappa/2$ curve, and the presence of the nILR. Nuclear spirals can propagate in two regions here: in the circle inside the nILR, and in the ring between the iILR and the oILR.

3.2 Constraints on the gravitational potential from the pitch angle

Although nuclear spirals can extend all the way to the galactic centre either when there is a sufficient central mass concentration or a MBH in the constant-density core, or when there is no constant-density core at all, their morphology differs in these two cases. Here I examine what are the shapes of nuclear spirals predicted by the linear theory, depending on the gravitational potential.

Formula (20) gives the pitch angle of the spiral, in which the wavenumber k is given by the dispersion relation (21). Thus the pitch angle i is a function of the gravitational potential (rotation curve), the pattern speed, and the speed of sound. When self-gravity in gas is neglected, it can be written as

$$\tan i = \frac{c}{R\sqrt{(\Omega + \kappa/m - \Omega_B)(\Omega - \kappa/m - \Omega_B)}} \quad (24)$$

There are some immediate consequences of this formula:

- the pitch angle is proportional to the sound speed in the isothermal gas: the higher the sound speed, the less tightly wound spiral one should expect,
- at radii where $\Omega - \kappa/m = \Omega_B$, i.e. at the limits beyond which the spiral cannot propagate, its pitch angle approaches infinity; thus in the $m = 2$ case the spiral unwinds in the vicinity of the ILR (see however Section 4 on how self-gravity in gas alters this conclusion).

Moreover, for a power-law rotation curve $\Omega = Ar^B$, the pitch angle at small radii approaches values

$$\tan i = \frac{c}{f(B)r\Omega} = \frac{c}{Af(B)}r^{-B-1}, \quad (25)$$

and therefore

- if a MBH is present in the galaxy centre ($B = -3/2$), then $\tan i$ approaches zero at small radii, and the spiral winds up infinitely,
- the same is true for any descending rotation curve ($B < -1$),
- for any rising power-law rotation curve ($-1 < B < 0$), $\tan i$ increases infinitely towards the centre, and the nuclear spiral unwinds in the innermost regions,
- in the particular case of constant rotational velocity in the innermost galactic regions ($B = -1$), the pitch angle remains also constant (logarithmic spiral).

3.3 Nuclear spirals for three representative rotation curves

In order to visualize the magnitude of the trends listed above, I calculated the value of the pitch angle and the shape of the nuclear spiral for three rotation curves (A , B , and C), representative to the distinctions made above. Rotation curve A has linear inner rise, and it represents the class of galaxies with solid-body rotation in their centres, i.e. galaxies with constant-density core. Rotation curve B represents galaxies with a MBH in their centres, and potentials with central mass concentration or density cusp: it is created by adding to the constant-density-core potential of rotation curve A a $10^8 M_\odot$ MBH in the centre. Rotation curve C is a pure power-law — it was constructed to represent curves that do not rise linearly in the innermost regions. These three representative rotation curves and their corresponding $\Omega - \kappa/2$ curves are presented in the top panels of Fig.2.

To generate these rotation curves, I used gravitational potentials based on the ones commonly assumed when modeling gas flow in barred galaxies (e.g. Athanassoula 1992, Piner et al. 1995, Maciejewski et al. 2002). There the axisymmetric part of the stellar potential consists of a bulge and a disc. The disc surface density follows the Kuzmin law

$$\sigma(R) = \sigma_0(1 + R^2/R_0^2)^{-3/2}. \quad (26)$$

Here I fixed σ_0 and R_0 to the values set by Athanassoula (1992), when she originally proposed this form of the potential. The bulge density follows the modified Hubble profile

$$\rho(r) = \rho_b(1 + r^2/r_b^2)^{-3/2}, \quad (27)$$

with ρ_b and r_b fixed to produce almost flat rotation curve with $v_{\text{circ}} \simeq 220 \text{ km s}^{-1}$ at the radii of interest. A $10^8 M_\odot$ MBH is added to this bulge when generating rotation curve B . For rotation curve C (no MBH), this bulge profile has been modified to take the form

$$\rho(r) = \rho'_b \frac{r'_b}{r} (1 + r^2/r'_b{}^2)^{-3/2}, \quad (28)$$

which gives power-law rise in the innermost regions. Parameters ρ'_b and r'_b have been fixed in order to match the general appearance of rotation curves A and C . The assumed pattern speed of the rotating potential is $36 \text{ km s}^{-1} \text{ kpc}^{-1}$, which places the corotation at 6 kpc.

The most striking conclusion from the top panel of Fig.2 is that rotation curves A (linear inner rise) and C (power-law) appear similar, but their corresponding frequency curves are diametrically different. Note also that the MBH modifies the $\Omega - \kappa/2$ curve at radii much larger than that of the turn of the rotation curve towards Keplerian rise (middle column of Fig.2). Therefore phenomena like nuclear spirals, whose appearance depends primarily on the $\Omega - \kappa/2$ curve, may be able to indicate the presence of the MBH in cases where traditional methods based on the rotation curve still need higher angular resolution to be conclusive.

The second from the top panels in Fig.2 show the pitch angle values derived for the nuclear spiral from the linear theory. The potential generating rotation curve A (left column of Fig.2) has two ILRs, and the nuclear spiral can propagate only between radii of these resonances. It does not extend to the galactic centre, and does not wind inwards to form any kind of nuclear ring. To the contrary, the spiral

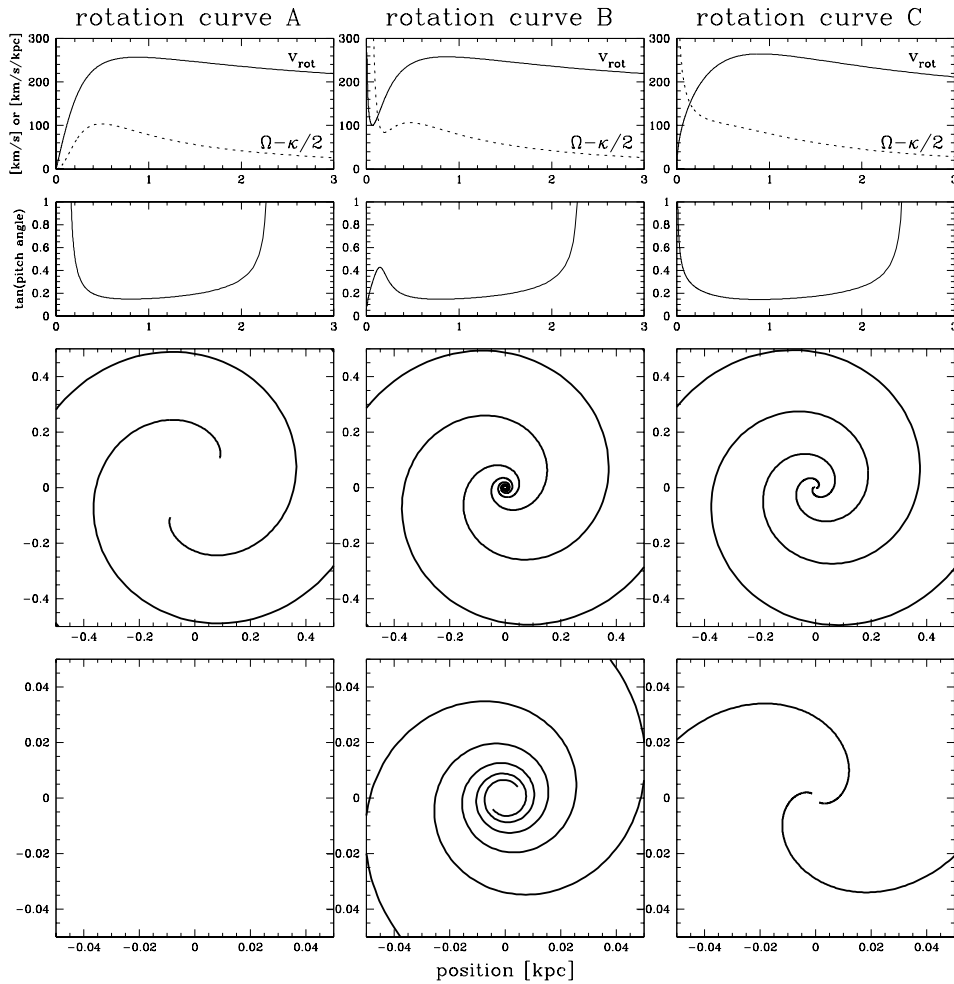


Figure 2. Characteristics of nuclear spirals for 3 representative rotation curves defined in Section 3.3. **Left column:** potential without a central MBH, and with constant-density core (rotation curve *A*). **Middle column:** potential with constant-density core, and a central MBH (rotation curve *B*). **Right column:** potential with a central density cusp (power-law), and no MBH (rotation curve *C*). Units on all horizontal axes are in kpc. **Top row:** Rotation curve (solid) and frequency curve (dotted). **Row second from the top:** tangens of the pitch angle of the spiral wave, calculated from (24) for sound speed in gas of 20 km s^{-1} . **Two bottom rows:** shapes of nuclear spirals calculated for pitch angles plotted above.

unwinds inwards, with an impression that it disappears at small radii, about 150 pc for the Athanassoula’s (1992) potential. It is unlikely that other physical processes can create a spiral inside the iILR boundary set by the linear theory, because in this region the galaxy rotates like a solid body, and winding due to differential rotation cannot take place.

The potentials generating rotation curves *B* and *C* (middle and right columns of Fig.2) have only one ILR, and the nuclear spiral can propagate all the way to the galactic centre there. However, the innermost shape of this spiral is diametrically different for those two potentials. If a MBH is present in the centre (or the central mass concentration is high enough that the rotation curve increases inwards), the spiral winds up inwards, which may eventually lead to the formation of a 10-pc scale ring around the MBH (middle column). On the other hand, if there is only a cusp in the stellar gravitational potential, causing the inner rotation curve to assume an increasing power-law shape (rotation curve *C*), then the nuclear spiral *unwinds* inwards, with the two arms pointing towards the galactic centre, and possibly forming

a bar-like feature. For the gravitational potentials used for the middle and right columns of Fig.2, the difference in the nuclear-spiral shape may not be distinct on a kpc scale (second from the bottom row of Fig.2), but it is clear on a 100-pc scale (the bottom row).

Note that the pitch angle may remain almost constant for most of the range within which the nuclear spiral can propagate (roughly between radii of 0.4 kpc and 2.0 kpc in Fig.2). This is because in these regions the rotation curve is almost flat, and $\Omega - \kappa/2$ is considerably above Ω_B . Then, $\Omega \pm \kappa/2$ is proportional to Ω , and in (24) one can neglect Ω_B , getting $\tan i \approx c/(R\Omega) = c/v \approx \text{const}$. This behaviour is consistent with the measured pitch angles (e.g. NGC 5248, Jogee et al. 2002).

The nuclear spirals observed in galaxies do not usually show two continuous spiral arms, but the arms get disrupted and lose continuity. Since the arm is a propagating density wave in gas, its extent depends on the duration of driver’s action. As I will show in Paper II, weak spirals can be driven by very small perturbations in the potential. These pertur-

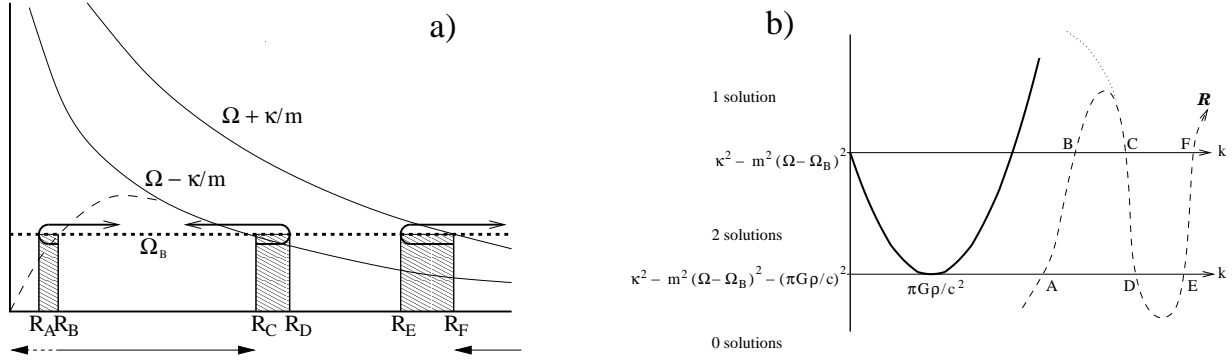


Figure 3. **a)** The frequency-radius diagram with the frequency curves $\Omega - \kappa/m$ and $\Omega + \kappa/m$ marked by solid lines. The dashed extension marks the possible behaviour of the $\Omega - \kappa/2$ curve at small radii. The dotted horizontal straight line represents the bar pattern speed Ω_B . Its intersections with the frequency curves define positions of the resonances. The permitted zones, where waves in gas can always propagate are indicated by arrows below the graph (dotted portion of the arrow is excluded from the permitted zone if $\Omega - \kappa/2$ follows the dashed line in the graph above). Shaded are penetration zones, where only waves in self-gravitating gas can propagate. Curved arrows in the graph mark propagation of the waves. **b)** Thick parabola marks the quadratic function of the wavenumber $k \geq 0$ on the left side of (16). Values of this function at $k = 0$, and at the minimum ($k = \pi G \rho / c^2$) are labeled. There may be 0, 1 or 2 solutions of (16), depending on how many times the abscissa intersects the parabola. Position of the abscissa depends on the radius at which (16) is evaluated: the dashed line shows how the abscissa shifts vertically, and the letters A-F along this line mark positions of the abscissa at radii $R_A - R_F$.

bations can be random, giving rise to discontinuous spiral structure. However, each spiral wave will still propagate according to the mechanism described above, with its pitch angle containing the same information about the potential as that of a continuous grand-design nuclear spiral.

4 NUCLEAR SPIRALS WITH SELF-GRAVITY IN GAS

4.1 Generation and propagation of waves

With self-gravity of gas included, (16) is a quadratic equation in $|k|$, and it is sufficient to analyze its solutions for $k > 0$. Mirror solutions for negative k represent waves propagating in the opposite radial direction. The quadratic function in (16) is shown in Fig.3b. It has real roots (solutions of eq.16) when its determinant is greater or equal to zero, i.e. when

$$(\Omega + \kappa/m - \Omega_B)(\Omega - \kappa/m - \Omega_B) \geq -(\pi G \rho_0 / mc)^2. \quad (29)$$

Since the term on the right of (29) is negative, one still gets real solutions everywhere in the regions where waves in not self-gravitating gas can propagate. Hereafter I call these regions the permitted zones. But waves in self-gravitating gas can also penetrate outwards of the ($m : -1$) Lindblad resonance located in Fig.3a at R_C (and also inwards of R_B if $m = 2$, see Section 3.1 for notes on multiple ILRs) as long as

$$\Omega - \kappa/m > \Omega_B - \frac{(\pi G \rho_0 / mc)^2}{\Omega + \kappa/m - \Omega_B}, \quad (30)$$

and they can penetrate inwards of the ($m : +1$) Lindblad resonance at R_F as long as

$$\Omega + \kappa/m < \Omega_B + \frac{(\pi G \rho_0 / mc)^2}{\Omega_B - (\Omega - \kappa/m)}. \quad (31)$$

Thus defined regions, shaded in Fig.3a, where waves can propagate in self-gravitating gas only, will be called hereafter the *penetration zones*. Inside these zones (16) has two solutions (see Fig.3b):

$$|k_{\pm}| = \frac{m}{c} \left(\frac{\pi G \rho_0}{mc} \pm \sqrt{\left(\frac{\pi G \rho_0}{mc} \right)^2 + (\Omega - \Omega_B)^2 - \frac{\kappa^2}{m^2}} \right). \quad (32)$$

The solution with '+' means larger $|k|$, i.e. shorter wavelength, and describes what is usually called short waves. The one with '-' describes long waves. On the other hand, in the permitted zones, where waves can propagate also in gas without self-gravity, (16) has only one solution: it is the short wave, because the long wave would have there $|k_-| < 0$, and thus no longer is a solution (see Fig.3b).

The result derived above allows for a qualitative description of the generation of waves by an external potential, and of their propagation in a mildly self-gravitating gaseous disc. For example, in the region around the ($m : -1$) Lindblad resonance, the long waves are generated at this resonance at R_C , and they propagate outwards towards R_D (left arm of the parabola in Fig.3b). There they get reflected (minimum of the parabola) as short waves (right arm of the parabola), which then freely propagate through the resonance inwards (the curved arrow in Fig.3a).

Since the ($m : -1$) Lindblad resonance is located inside the corotation radius, the wave-packets propagating around this resonance get advected in the direction of the rotation of the disc in the reference frame corotating with the potential. Long waves generated at the resonance at R_C propagate outwards, and therefore give rise to leading structures, while the reflected short waves propagate inwards, and therefore are trailing. Also trailing are the short waves reflected at R_E after being generated at the ($m : +1$) resonance. However, this time it is because the ($m : +1$) resonance is located outside the corotation, and waves propagating around it get

advection in the rotating frame in the direction opposite to the rotation of the disc. Short waves reflected at R_E are propagating outwards, and therefore the advection makes them trail. Note that if there is an additional $(2 : -1)$ resonance located at R_B , short waves related to it propagate outwards inside the corotation, and therefore the advection makes them lead. These are the only *short leading* waves predicted by this theory. In summary, short waves related to all $(m : -1)$ and $(m : +1)$ Lindblad resonances are trailing, except for a possible additional $(2 : -1)$ resonance (called the inner Inner Lindblad Resonance – iILR), where they are leading.

4.2 Quantitative estimates

Several interesting conclusions about the shape and extent of the spiral can be drawn from the solutions (32) for the wavenumber k . Waves in not self-gravitating gas can propagate inside the permitted zones, marked in Fig.3a by arrows under the graph. If self-gravity in gas is taken into account, the spiral can extend also into the penetration zones, shaded in Fig.3a. I estimate here the extent of these zones for the typically strongest $m = 2$ spiral, in a plausible galactic potential. For $m = 2$, the $(2 : -1)$ resonance is called the ILR, and the $(2 : +1)$ resonance – the OLR.

4.2.1 Extent of the penetration zones

In order to see differences in size between the penetration zones at various Lindblad resonances, one has to assume only some sensible values of the characteristic frequencies. I assume $\Omega_B = 20 \text{ km s}^{-1} \text{ kpc}^{-1}$, and a rotation curve that gives two ILRs, with $\max(\Omega - \kappa/2) = 70 \text{ km s}^{-1} \text{ kpc}^{-1}$. Let at this maximum $\Omega = 370 \text{ km s}^{-1} \text{ kpc}^{-1}$. The exact values are not important here, except for a large value of Ω compared to the other two frequencies above — this is seen both in observations and in numerical simulations (e.g. Schinnerer et al. 2002, Rautiainen et al. 2002). Moreover, let the density of the gaseous disc be $\rho_0 = 10 \text{ M}_\odot \text{ pc}^{-2}$, and the sound speed $c = 10 \text{ km s}^{-1}$. These values are set for reference only, and we will see how the solution depends on them. With such reference values, the self-gravity term in (30) and (31), $\pi G \rho_0 / 2c$, is about $7 \text{ km s}^{-1} \text{ kpc}^{-1}$. It is much smaller than the denominator in (30), and therefore the penetration regions around the ILR are rather small. The one around the inner ILR (iILR) is even smaller, because the value of denominator in (30) is very large there, and the $\Omega - \kappa/2$ curve rises there steeply. However, the situation is different around the OLR. There, the value of denominator in (31) gets closer to that of the self-gravity term, and the slope of the $\Omega + \kappa/2$ curve is small. Thus taking into account self-gravity shows that spirals around the OLR can extend much more inwards than the location of the resonance itself.

To take an example of a flat rotation curve, the long waves generated at the OLR can propagate inwards all the way towards the corotation when the self-gravity term, $\pi G \rho_0 / 2c$, approaches $\Omega_B / \sqrt{2}$. Since in this example the OLR is located at $1.71 R_{cr}$, where R_{cr} is the corotation radius, the penetration zone covers $0.71 R_{cr}$ inside the OLR for self-gravity of this strength. On the other hand, for the ILR located at $0.29 R_{cr}$ in this example, the same self-gravity allows the waves to penetrate outwards only up to $0.33 R_{cr}$,

making the penetration zone outside the ILR much smaller than that inside the OLR. This may suggest that the importance of self-gravity on the limits of wave propagation grows with galactic radius. Similar relations are true for any power-law rotation curve, though there the penetration zones corresponding to a given strength of self-gravity are slightly smaller in size than in the example of flat rotation curve considered here. Also, higher- m spirals develop larger penetration zones for a given self-gravity strength than the $m = 2$ spirals in this example.

From the form of the self-gravity term in (30) and (31) it is clear that the penetration regions grow in size with increasing gas density ρ_0 or decreasing speed of sound c . Moreover, the size of the penetration zone grows rapidly when the self-gravity term approaches Ω_B : in the example of a flat rotation curve, when this term reaches $\Omega_B/2$, the penetration zone around the ILR extends only from 0.29 to $0.31 R_{cr}$, but when it approaches Ω_B , (29) is always true, and self-gravity dominates. Since large amounts of gas are often present in centres of galaxies, with surface densities in the inner kiloparsec often a hundred or more times larger than the average densities (see e.g. Sakamoto et al. 1999), self-gravity may rule the propagation of waves around the ILR in this case. Then an interesting dichotomy among galaxies in their central morphology may develop: galaxies in whose central regions $\pi G \rho_0 / 2c < \Omega_B$ will have ILR-related spirals almost strictly confined to the permitted zone, while the same spirals in galaxies with $\pi G \rho_0 / 2c \approx \Omega_B$ in their centres will populate large penetration zones.

4.2.2 The shape of the spiral

Self-gravity in gas not only enlarges the regions where the spiral waves can propagate, it also changes the spiral morphology near the propagation limits. Propagation of waves in not self-gravitating gas is limited by the resonances, at which $|k| \rightarrow 0$. Therefore the pitch angle of the spiral increases there, and the arms open up and take almost radial direction (Fig.2, left column). When self-gravity is included, spirals can also propagate in the ‘penetration zones’ attached to the permitted zones, and shaded in Fig.3a. It can be seen from Fig.3b, as well as from (32), that at the external end of the penetration zone, the wavenumber k is independent of the potential, and takes the value $|k| = \pi G \rho_0 / c^2$. Thus the pitch angle, defined by (20), assumes there a certain value, which decreases with radius. At 10 kpc , where the OLR of a typical bar is usually located, the pitch angle at R_E for a two-arm spiral, with gas parameters in the disc defined above, is $i = 8^\circ$, much less than 90° for gas without self-gravity, and even still within the linear regime. For the ILR, which is typically located at some 2 kpc , this angle increases to 20° . Thus the self-gravity correction is (predictably) very strong in the vicinity of resonances, and it also increases with galactic radius. On the other hand, if it is calculated at the maximum of the $\Omega - \kappa/2$ curve, the correction is small. For the parameters of the disc assumed above, the term from the external potential in (32), $\sqrt{(\Omega - \Omega_B)^2 - \kappa^2/m^2}$, has a value of $180 \text{ km s}^{-1} \text{ kpc}^{-1}$, compared to the self-gravity correction, $\pi G \rho_0 / 2c = 7 \text{ km s}^{-1} \text{ kpc}^{-1}$. Thus the pitch angle gets corrected from 6.3° to 6.1° . Small value of this correction shows that although self-

gravity drastically changes solution at the resonances, it is of rather minor importance in the regions between the resonances, where waves can propagate.

Again, to take an example of a flat rotation curve, if self-gravity were to dominate the solution for the pitch angle at radii above 80% of the ILR radius, then it is required that $\pi G\rho_0/2c > 1.3\Omega_B$. Thus even if self-gravity leads to extensive penetration regions around the ILR, the morphology of the spiral does not change significantly in the permitted zones. However, before $\pi G\rho_0/c$ becomes greater than κ , i.e. before the global gravitational instabilities set in, the self-gravity term may assume values approaching the term $\sqrt{(\Omega - \Omega_B)^2 - \kappa^2/m^2}$ from the external potential throughout the permitted zone. The disc in the example above becomes unstable when $\pi G\rho_0/2c > 150 \text{ km s}^{-1} \text{ kpc}^{-1}$, which is almost equal to the value that the term from the external potential in (32) reaches at the tip of the $\Omega - \kappa/2$ curve. Thus for discs close to gravitational instability, the solution for the spiral can be significantly modified by self-gravity throughout the whole range where the wave propagates.

Thus for two-arm nuclear spirals which are related to the ILR, four different regimes of morphology and dynamics can be singled out within this linear theory, depending on the strength of self-gravity in gas:

- $\pi G\rho_0/2c < \Omega_B$: nuclear spirals confined to permitted zones, effects of self-gravity for the shape of the spiral are negligible,
- $\pi G\rho_0/2c \approx \Omega_B$: in addition to permitted zones, nuclear spirals fully populate penetration zones, but within the permitted zones the morphology of the spiral remains well described with self-gravity in gas neglected,
- $\Omega_B < \pi G\rho_0/2c < \kappa/2$: with the self-gravity term growing, solution for the spiral gets modified deeper in the interior of the permitted zone,
- $\pi G\rho_0/2c \geq \kappa/2$: gaseous disc becomes gravitationally unstable.

5 DISCUSSION

Linear analysis of nuclear spirals performed here for realistic galactic potentials can provide us with abundant information about the origin of the spirals as well as the shape of the potential in particular galaxies. The most striking fact about the nuclear spirals is their common appearance: recent high-resolution observations indicate that they extend continuously from kiloparsec scales inwards down to the resolution limit. According to the linear theory, this is possible only when the $\Omega - \kappa/2$ curve takes values sufficiently large at all radii where the spiral appears. Otherwise discontinuity in the spiral is expected. On the other hand, it has been often assumed that the typical rotation curve for a disc galaxy has a linear rise in its inner part. As I showed in Section 3, the linear rise means $\Omega - \kappa/2 \equiv 0$, so it prevents the nuclear spirals from propagating in the innermost regions of galaxies, contrary to what is observed. Other mechanisms to form the nuclear spiral are also unlikely to work there, since the linear rise of the rotation curve means no differential rotation, essential in the formation of the spiral.

How to explain this contradiction? Note that the $\Omega - \kappa/2$ curve is a derivative of the rotation curve, and at small radii it is very sensitive to the form of the underlying gravitational

potential: in particular it is more sensitive to the variation of the rotation curve's shape than to its value. Two rotation curves that fit a given set of observed data equally well can generate diametrically different $\Omega - \kappa/2$ curves. Consider for example rotation curves *A* and *C* (left and right panels of Fig.2): curve *A* reaches linear inner rise (equivalent to solid-body rotation), while curve *C* approaches a power-law in the inner part. They both may fit a given set of observed data equally well, but their corresponding $\Omega - \kappa/2$ curves are diametrically different: rotation curve *C* generates an $\Omega - \kappa/2$ curve which rises monotonically inwards, while rotation curve *A* forces the $\Omega - \kappa/2$ curve to decrease to zero at small radii (see Maciejewski 2003 for further discussion). Thus out of these two rotation curves, nuclear spiral extending to the innermost regions of the galaxy can form only for rotation curve *C* (power law). This proposition is consistent with fits to surface-brightness profiles of disc-galaxy nuclei, that show very good agreement with power-law profile (Balcells et al. 2001). For a power-law luminosity profile, the rotation curve is also a power law.

Since the observed nuclear spirals often extend continuously inwards from kiloparsec scales down to the resolution limit, the linear rise of innermost rotation curves in these galaxies becomes unlikely. Galaxies either usually don't have constant-density cores, or their potential is dominated by the gravity of the central MBH or mass concentration. Thus a linear rise of the central rotation curve, although a good approximation to the data, may not properly reflect the mass distribution and the dynamics in the inner parts of galaxies. Special care has to be taken when the presence and the positions of resonances are deduced from the observed rotation curve. Streaming motions and resolution effects, like beam smearing, give the impression of a linear rise in the central parts, which unavoidably implies the presence of an inner ILR.

In section 4, I showed that the role of self-gravity in gas increases with radius, and it is likely larger at the OLR than at the ILR. Self-gravity decreases the pitch angle of the spiral at the limit of the penetration zone (the *Q*-barrier), which for the penetration zone related to the OLR can give an appearance of a spiral not winding onto a ring inside it, but simply discontinuing inwards. The morphology of Mrk 590 (Pogge & Martini 2002) on the scale of a few kpc can have such an origin.

There is another structure of interest related to induced density waves, this time at the innermost radii, close to the sphere of influence of a MBH. If the frequency curve in a given galaxy takes the form from Fig.1d, then in addition to the nuclear spiral between the iILR and the oILR, a nuclear mini-spiral may form inside the nILR (Fukuda et al. 1998). It can be seen in Fig.2 (see also Maciejewski 2003), that this spiral extends further than the MBH's sphere of influence, and therefore can serve as an indicator and mass estimator of the MBH. Note that such nuclear mini-spirals do not extend continuously outwards, and therefore cannot connect to the structures at larger radii. Structures on scales below 100 pc in NGC4151 and NGC 5273 (Pogge & Martini 2002, Martini et al. 2003a) can be indicative of such nuclear mini-spirals.

6 CONCLUSIONS

I considered here predictions of the linear theory of waves induced in gas by a rotating potential, when applied to realistic and commonly assumed galactic potentials. Density waves in this theory give rise to nuclear spirals observed in the majority of disc galaxies. On images from the Hubble Space Telescope these spirals can be traced to approach the nucleus up to the resolution limit. This indicates that linearly rising inner rotation curves are rather an exception than the rule in galaxies, since otherwise they would prevent nuclear spirals from reaching the galactic centre. If the potential has a MBH in its centre, or mass concentration high enough, then the nuclear spiral winds tightly around the centre. For a potential with lesser mass concentration, like those characterized by a rising power-law rotation curve, nuclear spiral should unwind towards the centre, forming a bar-like structure in the innermost parts of the galaxy. Throughout the extent of the spiral its pitch angle is proportional to the velocity dispersion of the gas clouds. Self-gravity in gas significantly modifies the value of the pitch angle near resonances. This effect is stronger at larger radii. The zones where nuclear spirals can propagate get significantly enlarged when the self-gravity term, $\pi G\rho/mc$, approaches the pattern speed of the rotating potential. Departures from this linear picture will be studied in Paper II.

ACKNOWLEDGMENTS

I wish to thank Lia Athanassoula and Paul Martini for enlightening discussions, and the anonymous referee, whose comments helped to improve the clarity of this paper. I acknowledge the post-doctoral fellowship from Osservatorio Astrofisico di Arcetri, where most of this research has been done.

REFERENCES

- Athanassoula E., 1992, MNRAS, 259, 345
 Balcells M., Domínguez-Palmero L., Graham A., Peletier R. F., 2001, in Knapen J. H. et al., eds, ASP Conf. Ser. Vol. 249, The Central kpc of Starbursts and AGN: The La Palma Connection. Astron. Soc. Pac., San Francisco, p.167
 Binney J., Tremaine S., 1987, Galactic Dynamics. Princeton Univ. Press, Princeton
 Dehnen W., Binney J., 1998, MNRAS, 294, 429
 Elmegreen B. G. et al., 1998, ApJ, 503, L119
 Englmaier P., Shlosman I., 2000, ApJ, 528, 677
 Eskridge P. B. et al., 2000, AJ, 119, 536
 Fukuda H., Wada K., Habe A., 1998, MNRAS, 295, 463
 Goldreich P., Tremaine S., 1978, ApJ, 222, 850
 Goldreich P., Tremaine S., 1979, ApJ, 233, 857
 Jogee S. et al., 2002, ApJ, 575, 156
 Kormendy J., Gebhardt K., 2001, in 20th Texas Symposium on relativistic astrophysics, p.363
 Lin C. C., Shu F. H., 1964, ApJ, 140, 646
 Lin C. C., Shu F. H., 1966, Proc. Nat. Acad. Sci. USA, 55, 229
 Lindblad P. O., Jörsäter S., 1981, A&A, 97, 56
 Maciejewski W., 2003, in Boily C. M. et al., eds, EAS Publication Series Vol.10, Galactic & Stellar Dynamics. EDP Sciences, Les Illis, p.3
 Maciejewski W., 2004, MNRAS submitted (Paper II)
 Maciejewski W., Teuben P. J., Sparke L. S., Stone J. M., 2002, MNRAS, 329, 502
 Martini P., Pogge R. W., 1999, AJ, 118, 2646
 Martini P., Regan M. W., Mulchaey J. S., Pogge R. W., 2003a, ApJS, 146, 353
 Martini P., Regan M. W., Mulchaey J. S., Pogge R. W., 2003b, ApJ, 589, 774
 Montenegro L. E., Yuan C., Elmegreen B. G., 1999, 520, 592
 Piner B. G., Stone J. M., Teuben P. J., 1995, ApJ, 449, 508
 Pogge R. W., Martini P., 2002, ApJ, 569, 624
 Rautiainen P., Salo H., Laurikainen E., 2002, MNRAS, 337, 1233
 Regan M. W., Mulchaey J. S., 1999, AJ, 117, 2676
 Sakamoto K., Okumura S. K., Ishizuki S., Scoville N. Z., 1999, ApJ, 525, 691
 Schinnerer E., Maciejewski W., Scoville N., Moustakas L. A., 2002, ApJ, 575, 826
 Sellwood J. A., Wilkinson A., 1993, Rep. Prog. Phys., 56, 173
 Yuan C., Cheng Y., 1989, ApJ, 340, 216
 Yuan C., Cheng Y., 1991, ApJ, 376, 104
 Yuan C., Kuo C.-L., 1997, ApJ, 486, 750